

# Dynamical Reorganization of Synchronous Activity Patterns in Prefrontal Cortex–Hippocampus Networks During Behavioral Sensitization

Sungwoo Ahn<sup>1</sup>, Leonid L. Rubchinsky<sup>1,3</sup> and Christopher C. Lapish<sup>2,3</sup>

<sup>1</sup>Department of Mathematical Sciences and Center for Mathematical Biosciences, <sup>2</sup>Department of Psychology, Indiana University Purdue University Indianapolis, Indianapolis, IN 46202, USA and <sup>3</sup>Stark Neurosciences Research Institute, Indiana University School of Medicine, Indianapolis, IN, USA

Address correspondence to Sungwoo Ahn, Department of Mathematical Sciences, Indiana University Purdue University Indianapolis, 402 N. Blackford St., Indianapolis, IN 46202, USA. Email: ahnmath@gmail.com

**Neural synchrony exhibits temporal variability and, therefore, the temporal patterns of synchronization and desynchronization may have functional relevance. This study employs novel time-series analysis to explore how neural signals become transiently phase locked and unlocked in the theta frequency band in prefrontal cortex and hippocampus of awake, behaving rats during repeated injections of the psychostimulant, D-Amphetamine (AMPH). Short (but frequent) desynchronized events dominate synchronized dynamics in each of the animals we examined. After the first AMPH injection, only increases in the relative prevalence of short desynchronization episodes (but not in average synchrony strength) were significant. Throughout sensitization, both strength and the fine temporal structure of synchrony (measured as the relative prevalence of short desynchronizations) were similarly altered with AMPH injections, with each measure decreasing in the preinjection epoch and increasing after injection. Sensitization also induced decoupling between locomotor activity and synchrony. The increase in numerous short desynchronizations (as opposed to infrequent, but long desynchronizations) in AMPH-treated animals may indicate that synchrony is easy to form yet easy to break. These data yield a novel insight into how synchrony is dynamically altered in cortical networks by AMPH and identify neurophysiological changes that may be important to understand the behavioral pathologies of addiction.**

**Keywords:** Amphetamine, behavioral sensitization, hippocampus, neural synchrony, prefrontal cortex

## Introduction

Neural oscillations and synchrony are recognized as important mechanisms that underlie many physiological and pathological phenomena (Buzsáki and Draguhn 2004; Fell and Axmacher 2011). Neural signals may go in and out of synchrony due to insufficient synaptic strength to support perfect synchrony or temporal fluctuations of synaptic strength, variable input, noise, as well as any combination of these and other factors. The importance of understanding how oscillations become transiently synchronized and desynchronized has been recognized (Hurtado et al. 2004; Le Van Quen and Bragin 2007), and recently developed analysis techniques have made it possible to explore these processes (Park et al. 2010; Ahn et al. 2011).

One particularly powerful aspect of this approach is that the pattern of desynchrony can also be effectively described. This technique distinguishes between few long desynchronizations, numerous short desynchronizations, and a spectrum of possibilities in between, even if the average synchrony strength is not varied. This is especially important given that the synchrony described in a number of biological systems, including those described in the current study, is relatively moderate on

average (e.g., Jones and Wilson 2005; Adhikari et al. 2010). This type of weakly coupled oscillator spends a substantial fraction of time in the nonsynchronous state, thus the focus on the frequency and duration of desynchronization episodes allows observation of the network during its dominant state. This approach has been applied to neural oscillations in Parkinsonian patients, where elevated, but still moderate, synchrony coupled with numerous short desynchronized events is believed to contribute to the occurrence of motor symptoms (Park et al. 2010, 2011).

In the present study, we consider theta oscillations in prefrontal–hippocampal (PFC–HC) circuits of freely behaving rats. This band was selected as its role in cognitive functions mediated by these regions has been examined in depth (Hyman et al. 2005; Jones and Wilson 2005; Siapas et al. 2005; Adhikari et al. 2010; Sigurdsson et al. 2010). Moreover, perturbations in theta-band synchrony between these structures have been implicated in numerous neuropsychiatric disorders (Uhlhaas and Singer 2006) and rodent models of these conditions (Gruber et al. 2010; Gordon 2011). If synchronous dynamics are important to facilitate communication between different brain regions, then they may be altered in rodent models of neuropsychiatric disease.

Here, we explore how synchronized neural dynamics across these regions are progressively altered in time and in relation to ongoing behavior during sensitization. We used a regimen of repeated intermittent injections of the psychostimulant, D-Amphetamine (AMPH), that is well established to result in behavioral sensitization, an often-used model of both schizophrenia and addiction. AMPH evokes a number of alterations in the neurobiology of the PFC and HC and the behaviors they mediate (Robinson and Berridge 1993; Ujike 2002; Fletcher et al. 2007). As such, exploring how synchronized dynamics in these regions are altered during and after a sensitizing regime of AMPH will inform our understanding of the systems-level processes that are necessary to facilitate behavior and how they are altered in pathological states.

## Materials and Methods

### Animals

All animals were treated in accordance with the ethical standards outlined by the CCAC (UBC) and IACUC (IUPUI). Eight male Long-Evans rats (Charles River, Saint-Constant, QC, Canada) were allowed 1 week of acclimation upon arrival, and then microelectrode arrays were implanted. Four rats were treated with AMPH and 4 were treated with saline. Arrays were unilaterally implanted in both the medial PFC (anterior-posterior coordinate (AP) +3.2, medial-lateral coordinate (ML) +0.5, dorsal-ventral coordinate (DV) –3.0, relative to bregma) and the dorsal HC (AP –3.6, ML +2.0, DV –2.5, relative to bregma). Each

animal was anesthetized with isoflurane, placed into a Kopf stereotaxic frame, and surgery was performed. Probes were initially secured with Kwick-Sil (WPI, Sarasota, FL, USA) and then with dental acrylic that adhered to 5 skull screws. Each animal was given a minimum of 1 week for postoperative recovery before experiments were performed. Animals were first attached to the recording system and then placed into an environment that consisted of a 55-cm diameter white plexiglass arena surrounded by a 20-cm white plexiglass wall and allowed to freely explore. Each animal received a single intraperitoneal (i.p.) injection of either 1.0 mg/kg AMPH dissolved in 0.9% saline or an equal volume/weight of saline every other day (5 injections total) for the first 9 days of the experiment, referred to as the induction phase. This was followed by a 14-day incubation period during which the animals remained in their home cages, and received no injections. After the incubation period, animals were placed into the sensitization environment for 30 min and then given 1.0 mg/kg AMPH or saline i.p., referred to as the challenge phase. The pattern of induction, abstinence, and then drug challenge is designed to model the various stages of addiction from the initiation of drug taking behavior and ultimately craving and seeking of the drug after a period of abstinence (Robinson and Berridge 1993). Recording parameters were then optimized, and data were acquired for ~15 min before injection and then for ~45 min after injection for both saline- and AMPH-treated animals.

### Electrophysiology

Electrophysiological probes were fabricated using 25- $\mu$ m tungsten wires (California Fine Wires, Grover Beach, CA, USA) fed through silica tubing, yielding a separation of ~150  $\mu$ m between each recording site, and then secured to an EIB-27 micro (Neuralynx, Bozeman, MT, USA) via epoxy. In the PFC, wires were arranged in a 2  $\times$  8 array with the length of the array implanted along the anterior/posterior axis. In this region, half of the wires were internally referenced to an electrode in the PFC, and the other half of the wires were externally referenced to a stainless steel skull screw over the cerebellum. In the HC, the recording wires were arranged in a 1  $\times$  4 array with the length also running along the anterior/posterior axis. All wires in this region were externally referenced. Local field potentials (LFPs) were acquired with a 24-channel Neuralynx Cheetah recording system. LFPs were sampled at 30 303 Hz and amplified 2000 times, filtered between 0.01 and 1000 Hz and then down sampled to 947 Hz for analysis. At the end of each experiment, accurate placement of recording wires was confirmed via histology. Results for internally referenced and externally referenced wires in the prefrontal cortex were similar, and therefore for each animal, we report data from all possible pairs of externally referenced wires from the PFC and HC, yielding 8 different locations in the PFC and 4 different locations in the HC from each animal.

### Phase-Locking Analysis

Previously we, and others, have argued that analysis of synchronized dynamics in the phase domain is the most appropriate way to analyze neural signals that tend to be relatively weakly coupled (Lachaux et al. 1999; Varela et al. 2001; Hurtado et al. 2004; Le Van Quen and Bragin 2007). The presence of phase locking with a consistent phase lag indicates the presence of temporal coordination between signals (Pikovsky et al. 2001). In general, as the coupling strength increases from zero to relatively low values, synchrony will be observed in the phase domain while the amplitudes of oscillations remain uncorrelated (Pikovsky et al. 2001). While strong coupling leads to the coordination of both phases and amplitudes, weak coupling coordinates mostly phases. Thus, phase provides a sensitive and appropriate metric to explore the synchronous dynamics of relatively weakly synchronized systems with the benefit of detecting strongly coupled cases too.

Analysis was performed for LFPs from the PFC and the HC that were filtered in the theta (5–11 Hz) band. We followed analysis steps as in Park et al. (2010). Kaiser windowed digital FIR filter sampled at 947 Hz was used, and zero-phase filtering was implemented to avoid phase distortions. Phase was then extracted via Hilbert transform resulting in 2 signals;  $\varphi_1(t)$  and  $\varphi_2(t)$  (see Pikovsky et al. 2001; Hurtado et al. 2004). The following standard measure of the strength of phase locking

between these 2 signals was employed:

$$\gamma = \left\| \frac{1}{N} \sum_{j=1}^N e^{i\theta(t_j)} \right\|^2,$$

where  $\theta(t_j) = \varphi_1(t_j) - \varphi_2(t_j)$  is the phase difference, the  $t_j$  are the sampling points, and  $N$  is the number of data points to be considered. This phase-locking index varies from 0 (absence of phase locking) to 1 (perfect phase locking), but lacks information regarding the amplitude domain. This index is insensitive to amplitude fluctuations, but sensitive to the timing of activity in the given frequency band. However, this phase-locking index is not designed to describe the fine temporal structure of the dynamics, rather it provides an overall index of phase synchrony (Park et al. 2010; Ahn et al. 2011).

To assess the fine temporal structure of synchronous dynamics, we employed recently published methods based on the analysis of phase synchronization on short time scales via first-return maps (Park et al. 2010; Ahn et al. 2011). Briefly, whenever the phase of the reference signal crossed from negative to positive values, we recorded the phase of the other signal, generating a set of consecutive phase values  $\{\phi_i\}$ ,  $i = 1, \dots, N$ , where  $N$  is the number of such level crossing in the data. Thus,  $\phi_i$  represents the phase difference between 2 signals. Then,  $\phi_{i+1}$  versus  $\phi_i$  was plotted for  $i = 1, \dots, N - 1$ . Synchronous dynamics will predominantly appear as a cluster of points with the center at the diagonal  $\phi_{i+1} = \phi_i$  of the phase space. After determining the center of the cluster (i.e., determining the preferred phase difference between 2 signals at which they are predominantly locked), all values of the phases are shifted to a position with the center of the first region (quadrant; Fig. 1B). Thus, this approach is not concerned with the value of the phase shift between signals. Then, we consider how the system leaves the synchronization cluster and its vicinity, and how it returns back to synchronization by quantifying transitions between different regions of the  $(\phi_i, \phi_{i+1})$  space.

This phase space is then partitioned into 4 regions as illustrated in Figure 1B. While the system is in the first region, it is considered to be in a synchronized state as this is the preferred phase lag between the oscillators. Transitions outside of the first region reflect a desynchronized state. Thus, the synchronized state here is the one where the deviation from the preferred phase angle is  $< \pi/2$ . This value was arrived at empirically as it is not too small to allow for some moderate fluctuations of the phases, but not too large to prevent the unbounded deviation of one phase from the other so that some, potentially functionally important, correlations can be embedded in the signals. It also allows for symmetric partitioning of the phase space and definition of a few easy-to-compute transition rates (Ahn et al. 2011). Even though this partition is quite coarse, it allows for an inspection of the fine temporal details, as we will show below. Four resulting regions in the phase space are numbered in a clockwise manner (Fig. 1B), since this is the primary direction of the dynamics.

To explore the properties of synchronized dynamics, we computed the relative frequencies of desynchronization events of different durations. In the considered first-return map approach, the duration of a desynchronization event is the number of steps that system spends away from the first region minus one. For example, the shortest duration of the desynchronization event corresponds to the shortest path  $II \rightarrow IV \rightarrow I$  (Fig. 1B). This will correspond to the desynchronization length of 1 cycle (in other words, in 2 cycles, the phases are back in a locked state). This is shown in detail in Figure 1C, the preferred phase differences between 2 signals are between 0 and  $\pi/2$ , so that 2 phases are locked except the fourth crossing ( $\phi_4$  in Fig. 1C bottom). Figure 1C shows the examples of raw data and its corresponding filtered data at theta band from each brain region. The gray box in Figure 1C bottom shows desynchronization events with the duration of 1 cycle (in synch—out of synch—in synch). Examples of desynchronization events are presented in Figure 1D; length of 1 cycle (upper left), length of 2 cycles (upper right), and length of 3 cycles (lower left and right). Longer desynchronization events will have many different paths corresponding to them.

The distribution of durations of desynchronizations may be characterized by different parameters. Here, we look at the ratio of the

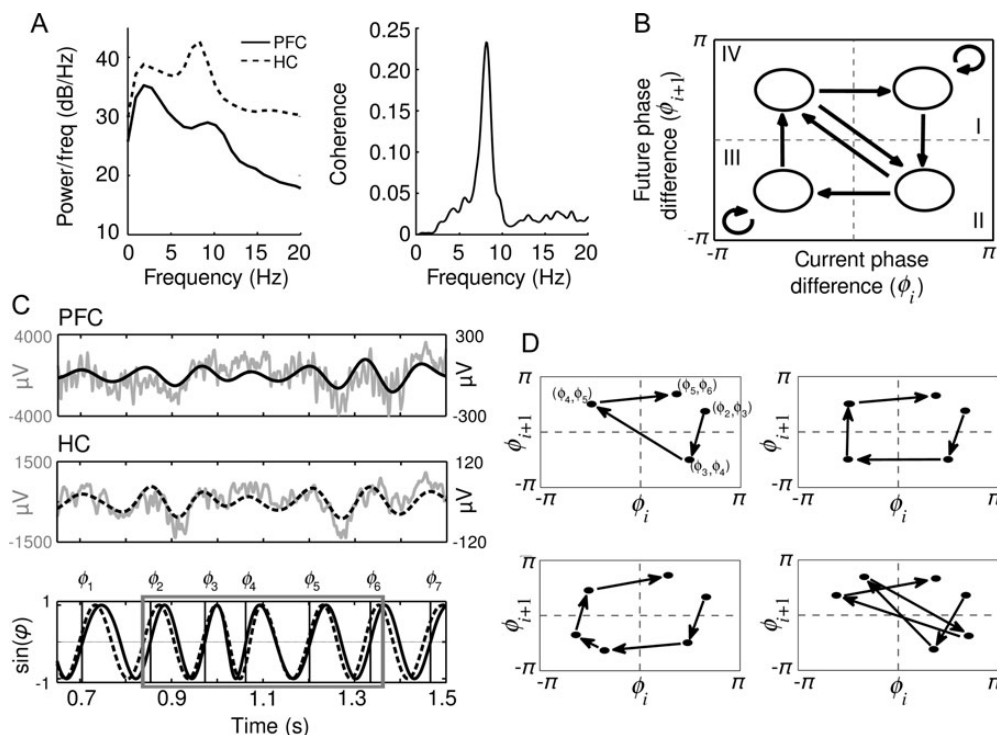


**Figure 1.** (A) Examples of PSD from PFC (solid line) and HC (dotted line) from a single animal during the postinjection epoch on Day 9 in the left panel and the corresponding MSC in the right panel. (B) Diagram of the  $(\phi_i, \phi_{i+1})$  first-return map. The arrows indicate all possible transitions from one region to another. The phase space is divided into 4 regions. While the system is in the first region, it is considered to be in a synchronized state. Dynamics outside of the first region will be called a desynchronized state. (C) Raw (light gray line) and filtered LFPs from the PFC (solid line) in the upper panel and the HC (dotted line) in the middle panel at the theta band. The bottom panel shows the sines of the phases of both filtered signals. The solid vertical lines indicate the phases of theta-band PFC LFP when the phases of theta-band HC LFP cross from negative to positive values. A gray box represents the desynchronization event with the duration of 1 cycle (in synch—out of synch—in synch). (D) Examples of the durations of desynchronization events of length of 1 cycle (upper left), length of 2 cycles (upper right), and length of 3 cycles (lower left and right). Note: the  $\phi_i$  above the bottom plot in (C) correspond to the point in phase space occupied at that time corresponding to the letters in the top left plot in (D).

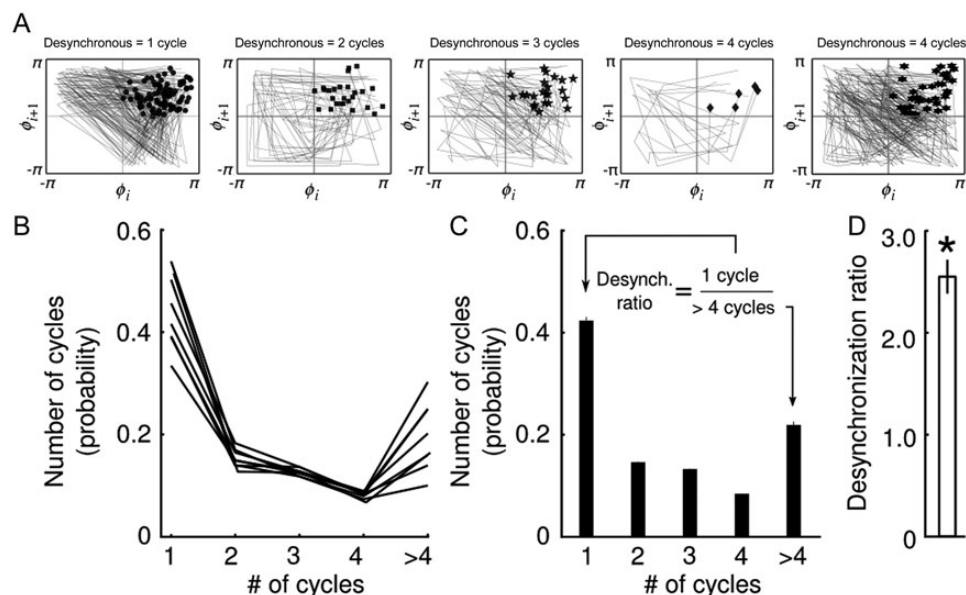


**Figure 2.** (A) Examples of the trajectories through phase space during each desynchronization event for a single animal on Day 9 during 4 min of the preinjection epoch. Each gray line shows a desynchronized event and is grouped with other desynchronized events of an equivalent durations ranging from a length of 1 (left) to >4 (right). The symbol in each plot represents the initial point of  $(\phi_i, \phi_{i+1})$  for the desynchronization event. (B) Line plots of the means of the durations of desynchronization events for each animal (saline and AMPH) during the preinjection epoch on Day 1. Note that 2 lines (the second and the third) are close to each other, so that they are not distinguishable. (C) The distribution of durations of desynchronization events for all animals corresponding to (B). In (B) and (C), the length of desynchronized events is presented as the number of cycles that a desynchronized epoch lasts before becoming resynchronized. Here, >4 cycles means the sum of the probabilities of all cycles whose lengths are >4. Note that all values in (B) and (C) are normalized relative frequencies (probabilities). Each bar in (C) and (D) plots the mean  $\pm$  SEM of the given distribution. (D) The distribution of the desynchronization ratio corresponding to (C). Asterisk represents one-sample *t*-test,  $P < 0.05$ .

relative frequencies of the desynchronizations lasting for one and longer than 4 cycles of oscillations. In other words, this is the ratio of the height of the first bin of the histogram of desynchronization durations to the fifth bin (Fig. 2C), which we refer to as the desynchronization ratio. It can take any nonnegative value. A smaller value identifies a bias toward longer desynchronization events, whereas a larger value identifies a bias toward short desynchronization events. This measure is different from the phase-locking index. Different values of the phase locking can yield the same value of desynchronization ratio, while different desynchronization values can accompany the same phase-locking index.

### Quantifying Coupling Between Behavior and Synchrony

To estimate the degree to which synchronized activity is related to behavior throughout the progression of sensitization, we determined if changes in synchronized activity tracked changes in locomotor activity. Locomotor activity was recorded via video camera, and the center of the animals' mass was detected in Noldus Ethovision (Leesburg, VA, USA). Locomotor activity was quantified as the cumulative distance traveled by an animal in either the pre- or postinjection epoch on a given day. The distance traveled was then normalized to the maximal value observed across all animals and days. The resulting number, called here the "locomotor activity index", varies between 0 (virtually no locomotor activity) and 1 (maximal locomotor activity). If synchronized activity between the PFC–HC influences locomotor output in a monotonous manner, then measures of oscillatory activity will either progressively increase or decrease throughout the course of sensitization. On the other hand, if synchrony and locomotor output are not directly related then no relationship should be detectable. To assess these possibilities, we used the values of the phase-locking index and desynchronization ratio from Day 1 (beginning of the induction phase), Day 9 (the end of the induction phase), and Day 23 (the challenge phase). The values of locomotor activity index and synchronized activity measures (phase-locking index and the desynchronization ratio) have 4 possible different trends over 3 considered days: Monotonous increase, monotonous decrease, U-shape, and inverted U-shape. If the values of locomotor activity index and phase-locking index follow either the same trend or exactly the opposite trend, then this pair of oscillations is marked by 1 (locomotion and phase locking are either correlated or anticorrelated, but are connected either way). If these values follow neither the same trend nor the opposite trend, then this pair of oscillations is marked by 0, which indicates a lack of correlation between phase locking and motor behavior. The same procedure was performed for the desynchronization ratio values. As a result, we have the distribution of the trend matching and nonmatching cases. We then computed the overall distributions of the pattern matching for each pair of recordings, then computed the probability of each of the 2 integers {0, 1}. In this context, we call the probability of having 1 a trend matching probability. The distributions were compared across 2 different animal groups (saline and AMPH) and 2 epochs (pre- and postinjection epochs) with 2-proportion *z*-test (also called difference in the proportions test) at the significant level. The significant increase of nonmatching and decrease of matching (or decrease of nonmatching and increase of matching) will point to alterations in the relationship between synchronized oscillatory activity and motor behavior. In other words, this trend matching probability provides an indication of how strongly the observed neural activity is correlated with motor behavior. We used the trend matching instead of a direct correlation between the locomotor activity index and synchronized activity measures, because the correlation is sensitive to the amplitude while trend matching is not. Moreover, the number of data points is small in our analysis, so that trend matching can effectively detect the changes of the relationship.

### Statistics

Analysis was performed in MATLAB (Mathworks, Natick, MA, USA) and R ([www.r-project.org/](http://www.r-project.org/)). Unless specified otherwise, all comparisons were first subjected to analysis of variance (ANOVA) testing with 3 possible factors: Groups (between subjects, saline, and AMPH),

injections (within subjects, pre, and post), and days (within subjects, Day 1, Day 9, and Day 23). Significance was set at  $\alpha = 0.05$ .

### Results

Figure 1A shows an example of the power spectral densities (PSDs) from the PFC (solid line) and HC (dotted line) during the postinjection epoch and corresponding magnitude-squared coherence (MSC). Note that there is the prominent peak in theta power in each brain region.

Inspection of the trajectories during each desynchronization epoch in the first-return map reveals that the majority of desynchronized episodes quickly return to the preferred phase (Fig. 2A). This phenomenon was also observed after plotting the distributions of the durations of desynchronization events for all animals (saline and AMPH), for example, on Day 1 prior to any injection (Fig. 2B). Figure 2C shows an example of the distributions of durations of desynchronization events for all animals on Day 1 during the preinjection epoch. We used the  $\chi^2$  goodness-of-fit test to detect nonuniform distribution of the durations of desynchronization events for each pair of wires for all animals (saline and AMPH), across Day 1, Day 9, and Day 23 for both the pre- and postinjection epochs, which resulted in >1000 pairs. The largest statistical *P*-value from these statistics was  $2.89e-3$  across all pairs, meaning that at least 1 of 5 bins in Figure 2C was reliably and highly significantly different from the other bins. We will look at this difference in detail below. In Figure 2C, most of the variability occurred in 1 cycle and >4 cycles, and for this reason these 2 points in the distribution were used to form a ratio to quantify the prevalence of short-/long-desynchronized events. We call this a desynchronization ratio (see also Materials and Methods). Figure 2D shows an example of the desynchronization ratio corresponding to Figure 2C. Note that the distribution of the desynchronization ratio in Figure 2D was computed as the mean of the distribution of the desynchronization ratios [1 cycle/(>4 cycles)] for each pair of wires, so that it was not directly derived from the means of the first and fifth bins in Figure 2C. Recall that the desynchronization ratio can be any nonnegative number where a smaller value identifies a bias toward longer desynchronization events, while a larger value identifies a bias toward short desynchronization events (see Materials and Methods). In our analysis, we will focus on this measure as well as the phase-locking index  $\gamma$ .

### Short Desynchronization Episodes Prevail in Dynamics of Theta Rhythm

No difference between saline and AMPH animals was observed in the preinjection epoch on Day 1 for  $\gamma$  ( $F_{1, 138} = 0.32$ ,  $P > 0.05$ ; Fig. 3C) or the desynchronization ratio ( $F_{1, 138} = 0.27$ ,  $P > 0.05$ ; Fig. 3D). In each animal, we observed that the PFC–HC network is engaged in weakly synchronized dynamics with a very specific temporal patterning of synchrony during the preinjection period, which is biased towards short periods of desynchronization.

Since the distributions of the durations of desynchronization events were significantly different from the uniform distribution for 5 bins for each pair of wires for both saline and AMPH animals on Day 1 during the preinjection epoch (see above), we performed additional analysis to determine which length of cycles was significantly different from others. To find the general patterns of the durations of desynchronization

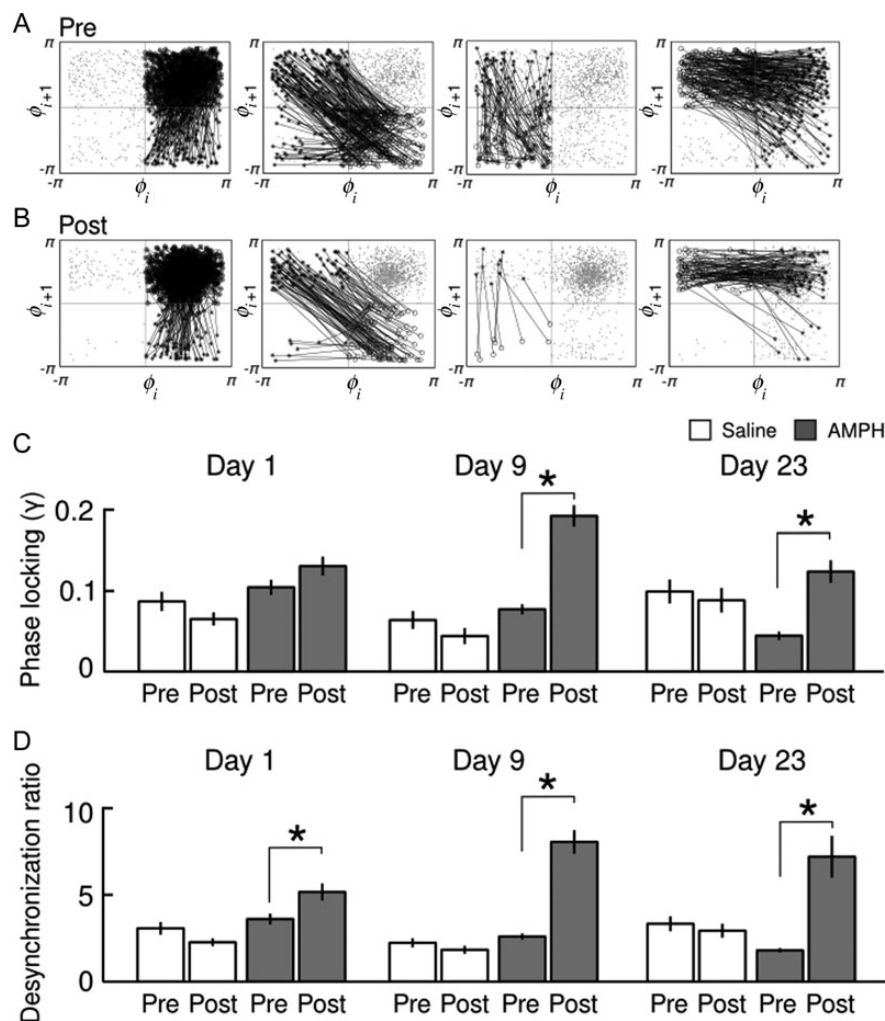


**Figure 3.** (A) An example of the first-return map for a single animal on Day 9 during the preinjection epoch for 4 min (same data as in Fig. 2A). All 4 first-return maps have the same data points (gray circles), but each subplot presents the evolution of points from 1 region. If a point evolves from one region to another region, then we represent it as  $\circ-\ast$ . If a point evolves within the same region, then we represent it as  $\circ-\circ$ . Thus, each plot shows the transitions from a corresponding part of the phase space. Note that most points in II moved to IV and most points in IV moved to I. Moreover, most point in III moved to IV. These transitions implied the high probability of short desynchronization events as they are the shortest possible path through the phase space. (B) An example of the first-return map during the postinjection epoch (the same pair of wires as in (A) for 4 min). The columns in (A) and (B) show the trajectories through each phase space before and after AMPH injection. The difference in the patterns of the trajectories across treatments was especially prominent in the second, third, and fourth columns in (A) and (B), which lead to fewer long desynchronizations after AMPH injection. (C and D) The phase-locking index  $\gamma$  and the desynchronization ratio for saline and AMPH animals during the pre- and postinjection epochs on Day 1, Day 9, and Day 23 at the theta band. The white and gray bars represent the saline- and AMPH-injected animals, respectively. Each bar plots the mean  $\pm$  SEM of the given distribution. (C) Distributions of  $\gamma$ . (D) Distributions of the desynchronization ratio. Asterisk represents Tukey's LSD,  $P < 0.05$ .

events on Day 1 during preinjection epochs, we pooled the data of the saline and AMPH animal groups. We reliably observed that the probability of desynchronizations lasting for 1 cycle was higher than that of desynchronizations of all other cycles, and this was confirmed statistically for all possible pairwise comparisons (1-sided paired  $t$ -test;  $t_{(278)} > 1.75e+1$ ,  $P < 3.29e-47$ ; Fig. 2B,C). Moreover, the desynchronization ratio [1 cycle/( $> 4$  cycles)] was also significantly higher than 1 (1-sided 1-sample  $t$ -test against 1;  $t_{(139)} = 8.82$ ,  $P = 2.11e-15$ ; Fig. 2D), which shows the prevalence of short (although, potentially numerous) desynchronization events. This prevalence was observed not only in intact animals, rather it persisted in all animals at all recordings episodes on the average and in each animal individually. Regardless of the treatment group, day of observation, or pre-/postinjection epoch, the short desynchronization events were dominant in the PFC-HC

network. Overall, for all the data we considered here, the probability for the mode of the distribution of desynchronization events to be at 1 cycle is 91.86%. The relatively high values of desynchronization ratios (see Fig. 3D) also point to the prevalence of short desynchronizations.

To assess the robustness of our observations with respect to small variations of bandwidth and the central frequency of the theta band, we performed the exact same data analysis as described above for a slightly changed bandwidth (6–10 Hz) and for the band with shifted central frequency (6–12 Hz). At these new frequency ranges, we observed that our results were preserved. The probabilities of short desynchronization (1 cycle of oscillations) were significantly higher than other durations regardless of conditions (groups, injections, and days) for 6–10 and 6–12 Hz bands too. This supports the finding that short desynchronizations robustly dominate synchronized neural dynamics.

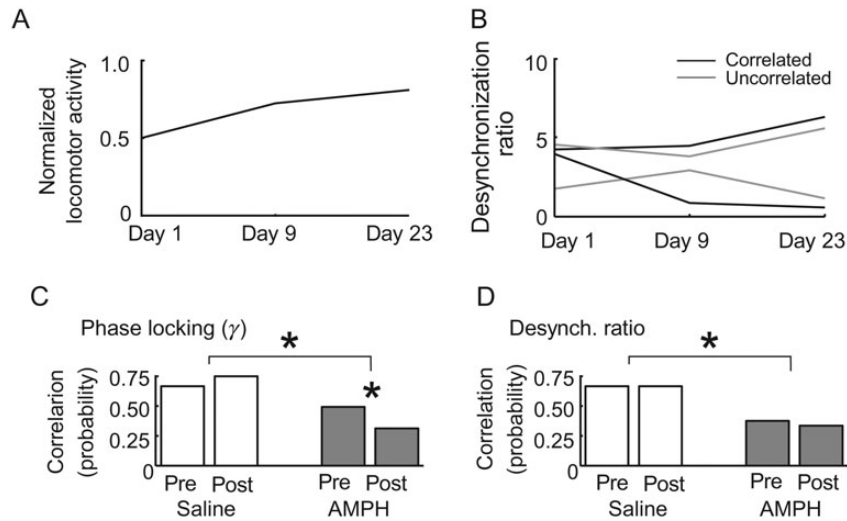


**Figure 4.** Trend matching of synchronized neural activity and motor behavior. (A) An example of locomotor activity index for 3 different days. (B) Examples of desynchronization ratio for 3 different days. When the locomotor activity index and desynchronization ratio show the same (or opposite) patterns, we mark this pair by 1 as a potential correlation between neural activity and behavior [black lines in (B)]. When they show the different pattern, we mark the pair of signals by 0 as a potential absence of correlations between neural activity and behavior [gray lines in (B)]. See *Materials and Methods* for details. (C and D) The trend matching results: The fraction of potentially correlated signal pairs for different animal groups for both the pre- and postinjection epochs. The synchronized activity is characterized by the phase-locking index  $\gamma$  (C) and the desynchronization ratio (D). Asterisk represents 2-proportion z-test,  $P < 0.05$  or  $< 0.0125$  (see the text).

### Synchronized Dynamics Are Altered Throughout Sensitization

Figure 3A,B shows an example of the first-return map during the pre- and postinjection epochs. As can be seen, almost all data points during the postinjection epoch (Fig. 3B) formed a cluster in the first region (I). Moreover, there were only few points moving either from II to III or from IV to II. This indicates shorter desynchronization events and higher synchrony during the postinjection epoch (Fig. 3C on Day 9 for AMPH animals). Below we describe the results of statistical analysis of the changes in synchrony strength and pattern throughout sensitization experiments.

To compare the distributions of the phase-locking index ( $\gamma$ ) and the desynchronization ratio for saline and AMPH animals across 3 different days and during the pre- and postinjection epochs, we first employed a mixed design 3-way ANOVA. For the phase-locking index ( $\gamma$ ), there were significant main effects of animal groups ( $F_{1, 828} = 6.95$ ,  $P = 8.54e-3$ ; Fig. 3C), days ( $F_{2, 828} = 10.00$ ,  $P = 5.12e-5$ ; Fig. 3C), and treatments ( $F_{1, 828} = 68.2$ ,  $P = 5.82e-16$ ; Fig. 3C). There were also significant effects of interactions between animal groups and days ( $F_{2, 828} = 3.38$ ,  $P = 3.46e-2$ ; Fig. 3C), groups and treatments ( $F_{1, 828} = 10.25$ ,  $P = 1.42e-3$ ; Fig. 3C), days and treatments ( $F_{2, 828} = 8.84$ ,  $P = 1.58e-4$ ; Fig. 3C). For the desynchronization ratio, there were significant main effects of animal groups ( $F_{1, 828} = 6.53$ ,  $P = 1.08e-2$ ; Fig. 3D) and treatments ( $F_{1, 828} = 64.41$ ,  $P = 3.46e-15$ ; Fig. 3D). There were also significant effects of interactions between groups and treatments ( $F_{1, 828} = 7.89$ ,  $P = 5.10e-3$ ; Fig. 3D), days and treatments ( $F_{2, 828} = 6.51$ ,  $P = 1.57e-3$ ; Fig. 3D).

No significant main effects of days, injections, or interactions were observed in saline-treated animals for both  $\gamma$  and desynchronization ratio (Fig. 3C,D). For AMPH animals, a significant main effect of days ( $F_{2, 762} = 11.91$ ,  $P = 8.07e-6$ ; Fig. 3C), injection ( $F_{1, 762} = 73.42$ ,  $P < 2.e-16$ ; Fig. 3C), and an interaction between day and treatment ( $F_{2, 762} = 9.04$ ,  $P = 1.32e$

$-4$ ; Fig. 3C) were observed for phase-locking index  $\gamma$ . For the desynchronization ratio, there was no significant main effect of days ( $F_{2, 762} = 1.38$ ,  $P > 0.05$ ; Fig. 3D), but there was a significant main effect of injections ( $F_{1, 762} = 66.74$ ,  $P = 1.28e-15$ ; Fig. 3D) and an interaction between day and treatment ( $F_{2, 762} = 6.46$ ,  $P = 1.66e-3$ ; Fig. 3D). Therefore, we will focus our analysis on the phase-locking index  $\gamma$  and the desynchronization ratio for AMPH animal group below.

### Changes in the Pattern of Synchrony May Precede Changes in the Synchrony Strength

On Day 1,  $\gamma$  was increased slightly after injection relative to preinjection levels, but this increase was not significant (2-sided paired  $t$ -test;  $t_{(254)} = -1.75$ ,  $P = 8.07e-2$ ; Fig. 3C). However, significant difference was detected through the desynchronization ratio (2-sided paired  $t$ -test;  $t_{(254)} = -2.70$ ,  $P = 7.40e-3$ ; Fig. 3D). This implied that acute AMPH already induced changes in the fine temporal dynamics between these brain regions, while the overall synchrony level was similar.

### Phase-Locking Index and Desynchronization Ratio Peak at the End of the Induction Phase During the Postinjection, but not Preinjection, Epochs

In Figure 3C,D, both  $\gamma$  and the desynchronization ratio progressively decreased in each preinjection epoch in AMPH animals, as each pair-wise comparison during the preinjection epochs for AMPH was significantly different (2-sided paired  $t$ -test;  $t_{(254)} > 2.83$ ,  $P < 4.99e-3$  for the ratio, and  $t_{(254)} > 2.43$ ,  $P < 1.59e-2$  for  $\gamma$ ; Fig. 3C,D). In contrast, after injection of AMPH,  $\gamma$  peaked on Day 9 compared with the postinjection epochs in Day 1 and Day 23: Day 1 versus 9 (2-sided paired  $t$ -test;  $t_{(254)} = -3.47$ ,  $P = 6.05e-4$ ; Fig. 3C), Day 9 versus 23 (2-sided paired  $t$ -test;  $t_{(254)} = -3.54$ ,  $P = 4.79e-4$ ; Fig. 3C), but not for Day 1 versus 23 (2-sided paired  $t$ -test;  $t_{(254)} = -3.67e-1$ ,  $P > 0.05$ ; Fig. 3C). A similar pattern of activity was observed in AMPH animals for the desynchronization ratio, where it

peaked in the postinjection epoch on Day 9: Day 1 versus 9 (2-sided paired  $t$ -test;  $t_{(254)} = -3.44$ ,  $P = 6.86e-4$ ; Fig. 3D), but neither for Day 9 versus 23 (2-sided paired  $t$ -test;  $t_{(254)} = -6.14e-1$ ,  $P > 0.05$ ; Fig. 3D) nor Day 1 versus 23 (2-sided paired  $t$ -test;  $t_{(254)} = 1.56$ ,  $P > 0.05$ ; Fig. 3D).

#### *Injection of AMPH Increases Phase-Locking Index and Desynchronization Ratio Both at the End of the Induction Phase and at the Reinstatement*

For AMPH animals on Day 9 and Day 23, both  $\gamma$  and the desynchronization ratio robustly increased after injection relative to preinjection levels (2-sided paired  $t$ -test;  $t_{(254)} < -4.44$ ,  $P < 1.36e-5$  for the desynchronization ratio, and  $t_{(254)} < -5.32$ ,  $P < 2.26e-7$  for  $\gamma$ ; Fig. 3C,D). These values during the postinjection epoch were twice as large as those during the preinjection epoch.

#### *Phase-Locking Index and Desynchronization Ratio in Saline and AMPH Groups Are Different Even Before Reinstatement Injection*

No significant differences were observed comparing the preinjection periods of saline- and AMPH-treated animals on Day 1 and Day 9 (2-sided paired  $t$ -test;  $t_{(138)} > -6.53e-1$ ,  $P > 0.05$ ; Fig. 3C,D). However, a significant difference between saline- and AMPH-treated animals was observed prior to injection on Day 23 for both  $\gamma$  (2-sided paired  $t$ -test;  $t_{(138)} = 2.98$ ,  $P = 3.45e-3$ ; Fig. 3C) and the desynchronization ratio (2-sided paired  $t$ -test;  $t_{(138)} = 3.40$ ,  $P = 8.67e-4$ ; Fig. 3D).

As in the previous subsection, we slightly changed the frequency band to either 6–10 or 6–12 Hz. As before, we observed that all of our results were still preserved. This supports that the dynamics throughout sensitization were robustly altered in the theta band.

#### *Synchrony Becomes Decoupled From Behavior in Sensitized Animals*

Figure 4A,B shows examples of the temporal trends of locomotor activity index and the desynchronization ratio. The black and gray lines in Figure 4B represent the cases of trend matching and nonmatching cases (1 and 0 s, respectively) for an animal from the AMPH group (see Materials and Methods). Figure 4C,D shows the degree of trend matching [i.e., overall proportions (probabilities) of trend matching] during the pre- and postinjection epochs for saline and AMPH animals at the theta band.

We compared the difference in the probabilities of a trend matching for 2 different populations (between treatment groups or between pre- and postinjection epochs within a treatment group) by 2-proportion  $z$ -test. Here,  $H_0: P_x = P_y$  and  $H_A: P_x \neq P_y$ , where  $P_x$  and  $P_y$  are the probabilities of observing a trend matching in each of the 2 populations.

There were significant differences in the probabilities of a trend matching between saline and AMPH animals for both  $\gamma$  (2-proportion  $z$ -test,  $P = 1.74e-3$ ; Fig. 4C) and desynchronization ratio (2-proportion  $z$ -test,  $P = 2.01e-3$ ; Fig. 4D). We further performed 4 additional tests of differences in the probabilities of a trend matching between 2 animal groups during each epoch (pre- and postinjection epochs) and between pre- and postinjection epochs within the same animal group. Here, the significant level is set at  $\alpha = 0.0125$  (for the Bonferroni correction).

Figure 4C,D shows that there were no significant differences in the proportion of recordings exhibiting a trend matching between locomotor activity and  $\gamma$  or the desynchronization ratio between pre- and postinjection epochs for the saline group (2-proportion  $z$ -test,  $P > 0.0125$ ). On the other hand, there was a significant difference in the probabilities of a trend matching for  $\gamma$  between pre- and postinjection epochs for AMPH animals (2-proportion  $z$ -test,  $P = 2.86e-3$ ; Fig. 4C). Moreover, the significant difference in the probabilities of a trend matching between 2 animal groups during postinjection epochs for  $\gamma$  was observed (2-proportion  $z$ -test,  $P = 8.81e-4$ ; Fig. 4C).

The probabilities of a trend matching for the saline group during pre- and postinjection epochs were high ( $>0.6$  in Fig. 4C,D) for both  $\gamma$  and the desynchronization ratio. This implies that the locomotor activity index for the saline group had a substantial relationship with the strength and pattern of neural synchrony in PFC–HC brain regions. On the other hand, the trend matching for AMPH animals is relatively weak ( $<0.5$  in Fig. 4C,D) and is smaller than for saline animals. This suggests that the relationship between synchronized neural activity in the considered brain regions and motor behavior in saline animals is stronger than in AMPH animals. In other words, administration of AMPH decreases the degree to which synchronized dynamics in the PFC–HC networks is related to motor behavior. This is further confirmed by the significant changes in the analysis of trend matching for the phase locking of oscillations in both the pre- and postinjection epochs for AMPH, but not for saline, animals (see above).

## Discussion

### *Short Desynchronization Episodes Prevail in Theta Rhythm*

In the current study, average synchrony strength was detected prior to the analysis of the fine temporal structure, which is a prerequisite for using the first-return map approach to detect the fine temporal dynamics of synchrony. Using this approach, we observed that short desynchronized events were overwhelmingly the most prevalent and conversely the longer the desynchronized event, the fewer times it was observed. Note, that if synchrony is very strong, the prevalence of short desynchronization events may be not very surprising, since there may not be enough time left for long desynchronized episodes. Generally speaking, short desynchronizations do not necessarily dominate the dynamics of synchronized activity (Ahn et al. 2011). However, in our experiment, short desynchronizations were the most frequently observed in both amphetamine and control groups. This synchrony pattern coupled with the observation that the oscillations examined here are relatively weakly synchronous suggests that cortico-hippocampal networks favor a state of weak synchrony with frequent short desynchronizations in both intact and addicted brain.

To our knowledge, this is the first examination of the intermittent nature of synchronous dynamics in this system; however, there are a number of studies that observe changes in the strength of synchrony during behavioral tasks (Hyman et al. 2005; Jones and Wilson 2005; Womelsdorf et al. 2007; Benchenane et al. 2010). Recent studies of neural activity in the basal ganglia of Parkinsonian patients revealed a specific

fine temporal structure of the synchrony between spikes and LFPs in subthalamic nucleus with prevailing short desynchronizations (Park et al. 2010; Rubchinsky et al. 2012). The change in the frequency of short desynchronizations has been conjectured to be the mechanism that moves the basal ganglia networks closer to the boundary of synchrony at the rest state, so that presumably pathological (hypokinetic) episodes of synchrony are formed spontaneously (Park et al. 2011).

The dominance of short desynchronizations may constitute a generic feature of the networks examined in this and other studies (Park et al. 2011; Rubchinsky et al. 2012). Even though the functional significance of the observed distribution of the desynchronization events is not known, we can speculate on potential functional implications. Synchrony has been conjectured to be important for several phenomena, including facilitation of input selection and plasticity, binding, memory consolidation, coding (reviewed in Buzsáki and Draguhn 2004), as well as a mechanism for the modulation of neuronal interactions (Womelsdorf et al. 2007). In all of these cases, coordination of activity at each instant of time is apparently essential, thus the duration during which these systems are desynchronized may carry important functional implications and possibly indicate the intervals during which the presumed function of synchrony is likely to be absent.

Breaking down synchrony frequently for a short amount of time may lead to very different consequences compared with a few prolonged episodes. Numerous short epochs of desynchrony may imply that synchrony in these systems is not difficult, or energy expensive, to attain quickly. This would potentially provide the temporal resolution necessary to communicate the instantaneous and fluid aspects of cognition. At the same time, numerous short desynchronizations (as opposed to infrequent, but long desynchronizations) may potentially facilitate the formation and dissolution of neural assemblies. Short desynchronizations are likely to indicate that synchrony is easy to form yet easy to break, so that whenever a cell assembly must be formed to facilitate a particular function or task, short desynchronization dynamics may allow for a quick and efficient formation and break-up of such an assembly. Testing this possibility via computational modeling will be important to understand how synchronous dynamics affect the formation of neural assemblies.

### ***Amphetamine Changes the Strength and Temporal Pattern of Synchrony in Prefronto-Hippocampal Circuits***

Amphetamine injections affect both the patterns and strength of synchrony throughout the course of sensitization. No appreciable effects of a saline injection were observed throughout the sensitization regime, suggesting that the injection itself did not cause these changes. However, while the first amphetamine injection does not significantly elevate the strength of the synchrony, it induces the rearrangement of the temporal pattern of synchrony by increasing the number of short desynchronizations at the expense of the longer desynchronizations, without a significant effect on synchrony strength. Therefore, AMPH may initially alter the temporal patterning of synchrony, which may be very important functionally in the progressive remapping of neural circuits with repeated drug use even if overall synchrony strength is not changed. These data suggest that the analysis of the temporal structure of synchrony may be especially important to explore

the initial changes in systems level communication, as they occur in rodent models of addiction. Thus, this measure may provide a powerful tool to observe the progressive remapping of neural circuits and may yield critical insights into initial stages of this process.

Subsequent injections of AMPH lead to more substantial effects, where not only synchrony patterns, but also synchrony strength, are robustly altered. This suggests that repeated injections of amphetamine lead to a progressive reorganization of synchronous dynamics in PFC–HC circuitry as the same dose of drug increases both the phase-locking index and the desynchronization ratio to a greater extent. Altered synchronous dynamics persisted for a 2-week cessation period where there was no exposure to the drug or drug-paired environment leading to 2 effects. First, the strength of PFC–HC synchrony increases by a factor of 2 after injection. Second, the temporal patterns of synchrony are substantially altered, in that there are more short desynchronized episodes.

Numerous changes in neurobiology and behavior are observed following repeated administration of psychostimulants (Kalivas 2005). These neuroadaptations can persist beyond the initial pharmacological effects of the drug and have been observed for weeks following the last drug administration (Robinson and Becker 1986). Interestingly, the phase-locking index and the desynchronization ratio both show a decreasing trend during the preinjection epoch throughout sensitization, which becomes significant during the reinstatement phase. These data suggest that the neuroadaptive changes evoked by repeated AMPH injections, exposure to the drug-paired environment, or combination of these 2, remap PFC–HC synchrony such that phase locking is suppressed and the prevalence of short desynchronized events is reduced. Therefore, in the absence of the drug, the protracted consequences of the drug and exposure to drug-paired cues were found to be the opposite of those observed after each injection. This suggests that separate mechanisms mediate synchronous dynamics in the absence versus in the presence of drug. Further exploration of this phenomenon could have very important implications for understanding the addicted brain and may provide a physiological target to understand the persistent changes in neural synchrony that contribute to the probability of relapse.

While the neural systems and the experimental parameters employed in the current study are very different from subcortical networks in Parkinson's disease, a number of interesting parallels were observed. Increases in synchrony are observed after injection of AMPH and have also been observed to accompany Parkinsonian akinesia and rigidity, suggesting a role for excessive synchrony in each of these conditions. Furthermore, increases in the desynchronization ratio were observed with AMPH, and relatively high values of the ratio have also been suggested to be involved in the expression of Parkinsonian motor symptoms. In this way, both excessive synchrony and high desynchronization ratios may mediate the inability of these neural systems to effectively govern behavior.

### ***Amphetamine Decreases Correlation Between Synchronous Activity Patterns and Motor Behavior***

Correlations between theta power in the HC and movement have been observed previously (Vanderwolf 1971; Buzsáki 2005). Here, we find substantial correlations between changes in locomotor activity and changes in phase locking or the

desynchronization ratio throughout the injection regime in the saline group. However, this relationship was significantly decreased in the AMPH group. Collectively, these data show that the relationship between synchrony and behavior breaks down with repeated injections of AMPH. The decoupling of locomotor activity and synchrony may reflect the inability of these structures to engage supervisory control over behavior. Interestingly, decoupling was observed both in the pre- and postinjection epochs, implicating neuroadaptive processes, including learning and anticipation generated with repeated injection of the drug and not just an acute pharmacological effect. Moreover, decoupling of the behavior and synchrony was more pronounced in the desynchronization ratio than phase locking in the preinjection epoch, suggesting that persistent neuroadaptive changes may be more easily detected in the fine temporal structure of synchrony than its strength.

In conclusion, this study, to our knowledge, is the first to examine the fine temporal structure of neural synchrony in rodents and found that numerous short desynchronized epochs dominated synchronized neurodynamics in both saline and AMPH groups. We find that first injection of AMPH significantly affects temporal patterning of synchrony, but not its average strength. Both phase locking and the fine temporal structure of synchrony are altered in a similar manner with repeated injections of AMPH, with each measure decreasing in the preinjection epoch and robustly increasing after injection. Finally, decoupling between locomotor activity and synchrony was observed in AMPH, but not in saline, animals. Overall, these results indicate that after repeated injections of AMPH synchrony is easier to attain, but also easier to break. These results may be important to understand how synchrony is altered in this neural circuit, and how it ultimately contributes to the expression of the altered behavioral phenotype observed with repeated psychostimulant exposure.

### Funding

This study was supported by the Institute for Mathematical Modeling and Computational Sciences (IUPUI).

### Notes

The authors also wish to thank Dr James M. Hyman for helpful comments on the manuscript. *Conflict of Interest:* None declared.

### References

Adhikari A, Topiwala MA, Gordon JA. 2010. Synchronized activity between the ventral hippocampus and the medial prefrontal cortex during anxiety. *Neuron*. 65(2):257–269.

Ahn S, Park C, Rubchinsky LL. 2011. Detecting the temporal structure of intermittent phase locking. *Phys Rev E*. 84:016201.

Benchenane K, Peyrache A, Khamassi M, Tierney PL, Gioanni Y, Battaglia FP, Wiener SI. 2010. Coherent theta oscillations and reorganization of spike timing in the hippocampal-prefrontal network upon learning. *Neuron*. 66(6):921–936.

Buzsáki G. 2005. Theta rhythm of navigation: link between path integration and landmark navigation, episodic and semantic memory. *Hippocampus*. 15:827–840.

Buzsáki G, Draguhn A. 2004. Neuronal oscillations in cortical networks. *Science*. 304:1926–1929.

Fell J, Axmacher N. 2011. The role of phase synchronization in memory processes. *Nat Rev Neurosci*. 12(2):105–118.

Fletcher PJ, Tenn CC, Sinyard J, Rizos Z, Kapur S. 2007. A sensitizing regimen of amphetamine impairs visual attention in the 5-choice serial reaction time test: reversal by a D1 receptor agonist injected into the medial prefrontal cortex. *Neuropsychopharmacology*. 32(5):1122–1132.

Gordon JA. 2011. Oscillations and hippocampal-prefrontal synchrony. *Curr Opin Neurobiol*. 21(3):486–491.

Gruber AJ, Calhoun GG, Shusterman I, Schoenbaum G, Roesch MR, O'Donnell P. 2010. More is less: a disinhibited prefrontal cortex impairs cognitive flexibility. *J Neurosci*. 30(50):17102–17110.

Hurtado JM, Rubchinsky LL, Sigvardt KA. 2004. Statistical method for detection of phase locking episodes in neural oscillations. *J Neurophysiol*. 91(4):1883–1898.

Hyman JM, Zilli EA, Paley AM, Hasselmo ME. 2005. Medial prefrontal cortex cells show dynamic modulation with the hippocampal theta rhythm dependent on behavior. *Hippocampus*. 15(6):739–749.

Jones MW, Wilson MA. 2005. Theta rhythms coordinate hippocampal-prefrontal interactions in a spatial memory task. *PLoS Biol*. 3(12):e402.

Kalivas PW. 2005. How do we determine which drug-induced neuroplastic changes are important? *Nat Neurosci*. 8(11):1440–1441.

Lachaux JP, Rodriguez E, Martinerie J, Varela FJ. 1999. Measuring phase synchrony in brain signals. *Hum Brain Mapp*. 8(4):194–208.

Le Van Quyen M, Bragin A. 2007. Analysis of dynamic brain oscillations: methodological advances. *Trends Neurosci*. 30(7):365–373.

Park C, Worth RM, Rubchinsky LL. 2010. Fine temporal structure of beta oscillations synchronization in subthalamic nucleus in Parkinson's disease. *J Neurophysiol*. 103(5):2707–2716.

Park C, Worth RM, Rubchinsky LL. 2011. Neural dynamics in Parkinsonian brain: the boundary between synchronized and nonsynchronized dynamics. *Phys Rev E*. 83:042091.

Pikovsky A, Rosenblum M, Kurths J. 2001. Synchronization: a universal concept in nonlinear sciences. Cambridge (UK): Cambridge University Press.

Robinson TE, Becker JB. 1986. Enduring changes in brain and behavior produced by chronic amphetamine administration: a review and evaluation of animal models of amphetamine psychosis. *Brain Res*. 396(2):157–198.

Robinson TE, Berridge KC. 1993. The neural basis of drug craving: an incentive-sensitization theory of addiction. *Brain Res Rev*. 18(3):247–291.

Rubchinsky LL, Park C, Worth RM. 2012. Intermittent neural synchronization in Parkinson's disease. *Nonlinear Dyn*. 68(3):329–346.

Siapas AG, Lubenov EV, Wilson MA. 2005. Prefrontal phase locking to hippocampal theta oscillations. *Neuron*. 46(1):141–151.

Sigurdsson T, Stark KL, Karayiorgou M, Gogos JA, Gordon JA. 2010. Impaired hippocampal-prefrontal synchrony in a genetic mouse model of schizophrenia. *Nature*. 464:763–767.

Uhlhaas PJ, Singer W. 2006. Neural synchrony in brain disorders: relevance for cognitive dysfunctions and pathophysiology. *Neuron*. 52(1):155–168.

Ujike H. 2002. Stimulant-induced psychosis and schizophrenia: the role of sensitization. *Curr Psychiatry Rep*. 4(3):177–184.

Vanderwolf CH. 1971. Limbic-diencephalic mechanisms of voluntary movement. *Psychol Rev*. 78(2):83–113.

Varela F, Lachaux JP, Rodriguez E, Martinerie J. 2001. The brainweb: phase synchronization and large-scale integration. *Nat Rev Neurosci*. 2:229–239.

Womelsdorf T, Schoffelen JM, Oostenveld R, Singer W, Desimone R, Engel AK, Fries P. 2007. Modulation of neuronal interactions through neuronal synchronization. *Science*. 316:1609–1612.